Annales
Geophysicae

The properties and causes of rippling in quasi-perpendicular collisionless shock fronts

R. E. Lowe and D. Burgess

Astronomy Unit, Queen Mary, University of London, UK

Abstract. The overall structure of quasi-perpendicular, high Mach number collisionless shocks is controlled to a large extent by ion reflection at the shock ramp. Departure from a strictly one-dimensional structure is indicated by simulation results showing that the surface of such shocks is rippled, with variations in the density and all field components. We present a detailed analysis of these shock ripples, using results from a two-dimensional hybrid (particle ions, electron fluid) simulation. The process that generates the ripples is poorly understood, because the large gradients at the shock ramp make it difficult to identify instabilities. Our analysis reveals new features of the shock ripples, which suggest the presence of a surface wave mode dominating the shock normal magnetic field component of the ripples, as well as whistler waves excited by reflected ions.

Key words. Space plasma physics (numerical simulation studies; shock waves; waves and instabilities).

1 Introduction

The structure of high Mach number collisionless shocks, for the case where the angle θ_{Bn} between the upstream magnetic field and the shock normal is greater than 45° ("quasi-perpendicular"), is dominated by the processes of ion thermalization. Reflection of a fraction of the incident ions leads to a foot, ramp and overshoot structure with a highly anisotropic distribution in the foot and ramp. The waves driven by instabilities of this distribution eventually lead to thermalization. Simulations using a (spatially) one-dimensional hybrid model played an important role in explaining observations of the Earth's bow shock. Here "hybrid" refers to a simulation in which the ions are modelled using a set of particles and the electron response is modelled as a fluid. Comparison with observations at the Earth's bow shock, especially the ion thermalization process and weak electron heating, have validated the use of this type of model.

The first investigations of departures from one-dimensional structure were carried out by Winske and Quest (1988), who studied the role of waves and structure transverse to the normal using two-dimensional hybrid simulations of quasi-perpendicular shocks. They found that the anisotropic downstream ion distributions, created at the shock by reflection, produced waves broadly consistent with local linear theory. The ion perpendicular temperature anisotropy drives the Alfvén ion cyclotron (AIC) instability, and the plasma behaviour is essentially a quasi-linear relaxation of the distribution. Winske and Quest found that, locally, the wavelength of the parallel propagating waves in the downstream region agreed with the fastest growing mode predicted by linear theory.

At the shock ramp itself large amplitude structures in the density and all components of the magnetic field were seen propagating across the shock surface, and along the magnetic field direction – what we will call ripples in this paper. Winske and Quest found a large discrepancy between the wavelengths measured in the ramp and those predicted from linear theory. Of course, the applicability of linear theory at the ramp itself, where the plasma is highly inhomogeneous, is questionable. Winske and Quest suggested that the rippling was associated with the AIC instability, but modified by the effects of nonlinearity and inhomogeneity.

Thomas (1989) carried out a comparison of one-, two- and three-dimensional hybrid simulations which indicated that the overall shock thermalization process was not affected by the dimensionality of the simulation. However, it was noted that the amplitude of the structures within the ramp was reduced in the three-dimensional simulations, relative to that seen in the two-dimensional simulations. A more detailed study of the downstream plasma evolution seen in two-dimensional hybrid simulations was carried out by McKean et al. (1995). In these simulations waves driven by the AIC and mirror instabilities were seen, both depending on the perpendicular ion temperature anisotropy. The bunched gyrophase and highly anisotropic distributions just behind the shock were seen to relax rapidly within about 10 ion iner-

tial lengths. Thereafter, the downstream waves comprised of AIC and mirror modes at near marginal stability, as observed in the terrestrial magnetosheath.

The role of the reflected ions in the shock foot was investigated by Hellinger et al. (1996), who carried out three-dimensional hybrid simulations with sufficiently high resolution and low resistivity, to show whistler waves generated near the shock propagating upstream. If the shock front is the source of upstream whistlers, then observations of such waves (Fairfield, 1974; Orlowski and Russell, 1991; Orlowski et al., 1995) can be viewed as indirect evidence of transverse structure at the shock. Hellinger et al. noted that in their simulations whistlers propagated upstream in a direction out of the shock coplanarity plane (which contains the shock normal and upstream magnetic field), and were apparently driven by the reflected ions in the foot of the shock. Further investigations by Hellinger and Mangeney (1997) identified the gyrotropic gyrating ion beam instability (Wong and Goldstein, 1988) as the source of the obliquely propagating whistlers. Hellinger and Mangeney also presented an argument for a minimum Mach number required for rippling of the shock surface due to the AIC instability. However, there is still no resolution of the problem of the applicability of linear theory at the shock ramp, as noted by Winske and Quest.

In addition to the hybrid simulation studies discussed above, there are also studies using full particle (particle ions and particle electrons) simulation codes. These suffer the generic drawback that, for the same computational effort as a hybrid simulation, a smaller domain is simulated. Krauss-Varban et al. (1995) showed that upstream whistlers could be found in an implicit full particle simulation, supporting the assumption of Hellinger and Mangeney (1997) that they are only lightly damped. The most comprehensive study of the supercritical oblique shock using a two-dimensional full particle code is that of Savoini and Lembege (1994). They found rippling on roughly lower hybrid scale lengths at the shock front, and this was not affected by whether the upstream field was either in, or out of, the simulation plane. The simulation domain was relatively small in the transverse direction, but should, in principle, have shown any AIC associated waves; however, large amplitude rippling in the normal field component was not seen. The apparent discrepancy between these results and the two-dimensional hybrid results of Winske and Quest (1988) has not been investigated in detail, probably due to the fact that Savoini and Lembege (1994) simulated a shock with $\theta_{Bn} = 55°$, compared to the perpendicular and quasi-perpendicular shocks investigated by Winske and Quest (1988) and in this paper. The full particle simulation of a quasi-perpendicular shock by Krauss-Varban et al. (1995) does show rippling on a similar scale to the results of hybrid simulations.

In this paper we report the results of two-dimensional, high resolution, hybrid simulations, where we have carried out a detailed analysis of the shock ripples first reported by Winske and Quest (1988). We demonstrate a number of new features of shock ripples and argue that ripples may be caused by a wave mode which resembles a surface wave. It is clear that
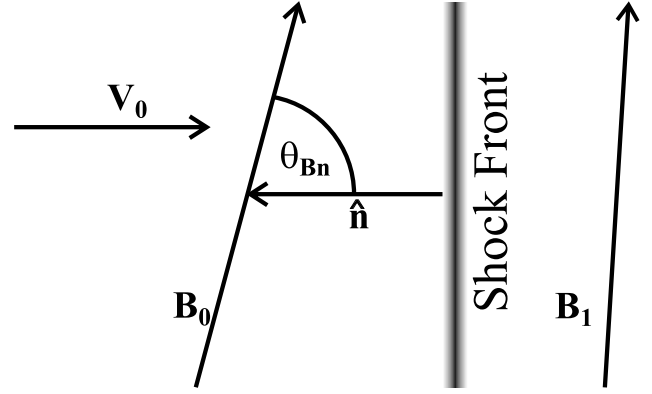

Fig. 1. The geometry of a collisionless shock in the normal incidence frame. The magnetic field B, inflow velocity V_0 and shock normal $\hat{n}$ are co-planar. In this reference frame, the geometry is such that V_0 and $\hat{n}$ are anti-parallel.

there is a substantial amount of free energy available at the shock front to excite such a mode, although we do not investigate the mechanism of the energy transfer. The shock transition is complicated by the flow across the boundary; however, our results indicate that the treatment of simpler surface problems, such as the study of tangential discontinuities by Hollweg (1982), are likely to be indicative of the more complicated shock solution. We find that our ripple properties would be consistent with this.

2 Simulation configuration

Our simulations use the CAM-CL hybrid code (Matthews, 1994). This models the plasma in a self-consistent manner as ion macroparticles and an inertialess electron fluid. The simulations are two-dimensional in space and three-dimensional in velocity. The choice of such a hybrid code means that electron physics is not accurately modelled at short scale lengths. In common with other hybrid shock simulations a small uniform resistivity is included which damps short wavelength oscillations. The hybrid simulation is also unable to accurately model electron scale waves and turbulence, which are seen in full particle simulation codes and which may affect the dynamics of ions as well as electrons. While electron inertial scales could be included by using a full particle code, the time and length scales associated with ion scale rippling are generally too long to be modelled in this way.

We generate a shock by reflecting homogeneous plasma moving at constant velocity off a stationary, perfectly conducting barrier, which provides a clean shock once the shock front is clear of the reflecting barrier. The plasma flows in from the left-hand x boundary and reflects at the right-hand x boundary; periodic boundary conditions are applied in the y direction. The geometry of the shock in the normal incidence frame is shown in Fig. 1. The shock, therefore, propagates from right to left, so that the inflow velocity of plasma into the simulation box, V_{in}, is less than the shock inflow velocity,
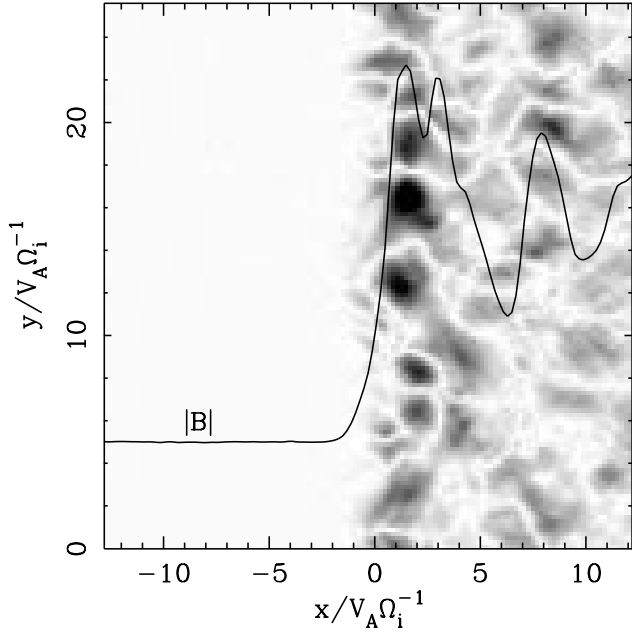
Fig. 2. A map of $|B_x|$ taken from a simulation with $\theta_{B_n} = 88°$ and $V_{in} = 4v_A$, giving $M_A \approx 5.7$. The maximum value of B_x is approximately $2B_0$ and the profile of $|\mathbf{B}|$ is superimposed.

V_0. Simulation units are normalised in terms of the upstream values of the magnetic field, B_0, the ion cyclotron frequency, Ω_i, and the Alfvén speed, v_A. Our simulations are run with a cell size $\Delta x = \Delta y = 0.2\, v_A\Omega_i^{-1}$, 360 cells in the x direction and 128 cells in the y direction, 50 ions per cell in the upstream, and a time step of $\Delta t = 0.01\, \Omega_i^{-1}$. The electron and ion upstream plasma beta are both 0.5.

The speed of the shock front was determined by using the mean value of the magnetic field over the y direction, $\langle B \rangle$. The shock front was considered to be located at the position where $\langle B \rangle$ reached twice the upstream value, i.e. $2B_0$. This actually corresponds to a point close to the foot of the shock, but the speed of this point is remarkably constant throughout a simulation, more so than if a point near the top of the ramp had been chosen. The shape of the shock was not constant, however, so the position and height of the overshoot vary slightly over time. Consequently, we have used the point where $\langle B \rangle = 2B_0$ as the origin for the x coordinate in the following discussion when quantities are described relative to the position of the shock front.

3 Overview of structure

According to the Rankine Hugoniot relations, since $\nabla \cdot \mathbf{B} = 0$, the shock normal magnetic field component, B_x, is constant across a one-dimensional shock. This means that any variations in B_x are purely the result of a two-dimensional structure in the shock front. Figure 2 shows a map of the B_x field component and the profile of the total magnetic field in the region of the shock for a simulation with $\theta_{B_n} = 88°$ and $V_{in} = 4v_A$, giving an Alfvén Mach number $M_A \approx 5.7$. In the

simulations, ripples are ion scale features at the shock front, which move along the shock surface. The waves associated with the rippling can be seen in the B_x component with a wavelength of 4 to 8 ion inertial lengths and an amplitude of around $2B_0$. These peaks also appear to be connected to the structure behind the shock, but not in any simple manner.

The ripples are most clearly visible in the shock normal component of the magnetic field, although there is also structure due to rippling in the other field components. Hodograms of B_x–B_y and B_x–B_z at the overshoot do not show any straightforward relationship between the components, in agreement with the results of Winske and Quest (1988).

We also ran an equivalent simulation in which the upstream magnetic field, $\mathbf{B}_0$, pointed out of the simulation plane. In this geometry the dimensionality of the simulation suppresses parallel propagating waves and structures, such as AIC waves and the shock ripples, so that the shock structure closely resembled that of a one-dimensional simulation, with little variation in the shock normal component B_x. The average profiles of the magnetic field and density were broadly similar in both simulations. This suggests that rippling does not significantly affect other properties of the shock, such as the shock width and the presence of the foot, ramp and overshoot.

4 Fourier analysis

We can apply Fourier analysis to characterise the properties of the B_x ripples and determine their dispersion relation. We do this by taking a time series of B_x field slices at a constant distance from the shock front. We take the Fourier Transform of this series of $y - t$ slices and square the result to obtain a power spectrum in $\omega - k$ space. The time domain is not periodic, so we apply a Bartlett windowing function in the t direction to reduce signal leakage. Our choice of analysing B_x at constant x means that we are looking at the projection of the two-dimensional $\mathbf{k}$ space on to the y direction transverse to the shock, and effectively parallel to the magnetic field.

Figure 3 shows $\omega - k$ power spectral maps for B_x at various positions relative to the shock front, with power plotted on a logarithmic scale. Upstream of the shock, there is no significant wave activity, and it is impossible to resolve a dispersion relation since any signal is lost in noise. The downstream power graph shows a peak at $\omega \approx 1.5\Omega_i$, although it is still difficult to resolve a dispersion relation. This is because we are effectively measuring $k_\parallel$, but if the actual dispersion relation does not depend only on $k_\parallel$, then for a given $k_\parallel$ waves over a range of $\mathbf{k}$ are sampled, and, hence, over a range of ω.

The wave activity in B_x within the shock front is considerably different from that outside, with significantly more power, and the peak at $\omega \approx 3.0\Omega_i$ being at a slightly higher frequency than for the downstream waves. There is also significantly more power at the overshoot than in the foot. Although the ripples in B_x look like "blobs" of field struc-
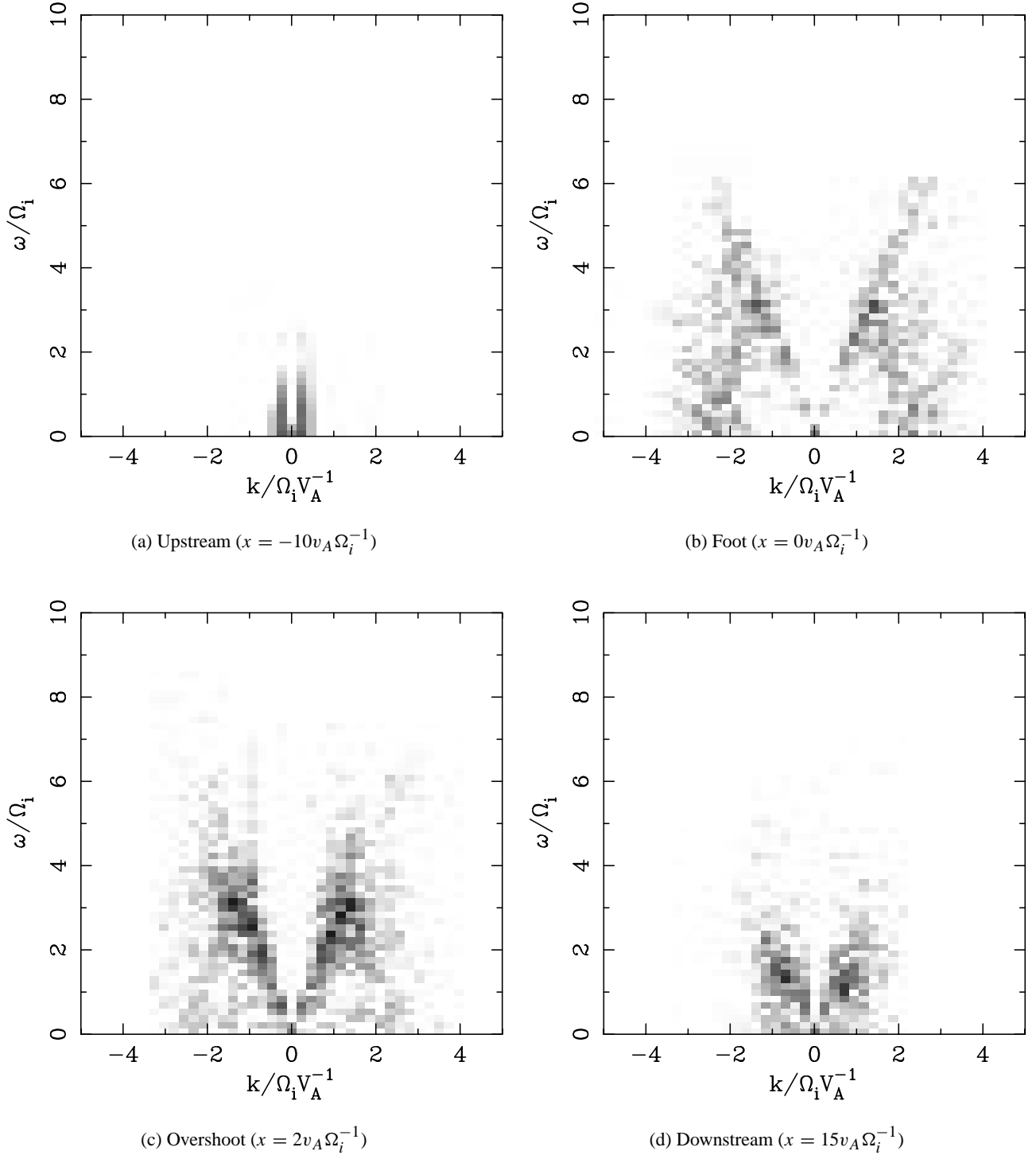
(a) Upstream ($x = -10 v_A \Omega_i^{-1}$)

(b) Foot ($x = 0 v_A \Omega_i^{-1}$)

(c) Overshoot ($x = 2 v_A \Omega_i^{-1}$)

(d) Downstream ($x = 15 v_A \Omega_i^{-1}$)

Fig. 3. The Fourier plots show the $\omega - k$ distribution of power for B_x field slices for the simulation with $\theta_{B_n} = 88°$ and $M_A \approx 5.7$. The high frequency and wave number regions of the Fourier transform, where there is very little power, are not shown. The power scale is identical on all four figures and is logarithmic, covering a factor of 1,000 in power.

ture, they actually show very clear wave mode properties. In Figs. 3b and c there is clearly a component of the power spectrum which shows a well-defined and linear dispersion relation, in contrast to the downstream spectrum. The sig-
nal remains clear up to around $|k| = 2.0 \Omega_i v_A^{-1}$. This value is higher than that for downstream waves, but it is approximately constant between the foot and the overshoot, despite the very different power to noise ratios. Figure 4 shows the
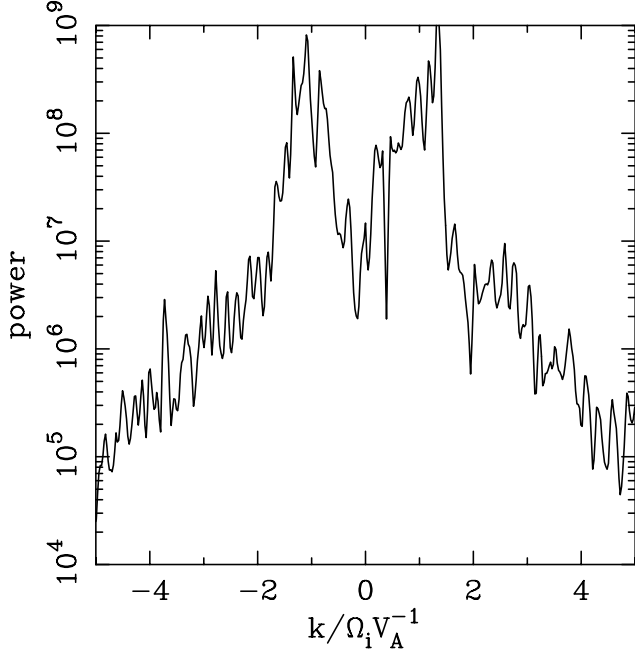
Fig. 4. Graph plotting the power in the Fourier Transform of Fig. 3c against k along the maximum power best fit dispersion relation.

Fig. 6. Fourier transform of the B_z magnetic field component for a field slice running along the shock overshoot ($x = 2v_A\Omega_i^{-1}$) of a $\theta_{B_n} = 88°$, $M_A \approx 5.7$ simulation.

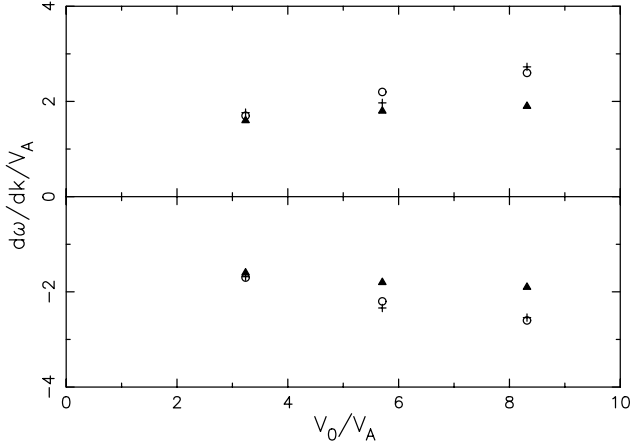**Fig. 5.** Chart correlating the speed of ripples at the overshoot to other significant wave speeds at $\theta_{B_n} = 85°$. The crosses correspond to the measured best χ^2 fit to the ripple speed, the open circles to the overshoot Alfvén speed and the solid triangles to the downstream Alfvén speed.

power along the best fit line for the dispersion relation at the overshoot in Fig. 3c, which suggests that this is a very high frequency cutoff. The region of maximum power at the overshoot corresponds to a wavelength of 4 to 8 ion inertial lengths, which agrees with the dominant scale of the ripples seen in the B_x field component in Fig. 2.

In order to examine the properties of this wave mode, we have carried out a series of simulations at different Mach numbers. For this set of simulations we have fixed $\theta_{Bn} = 85°$, but the results are representative of the whole quasi-

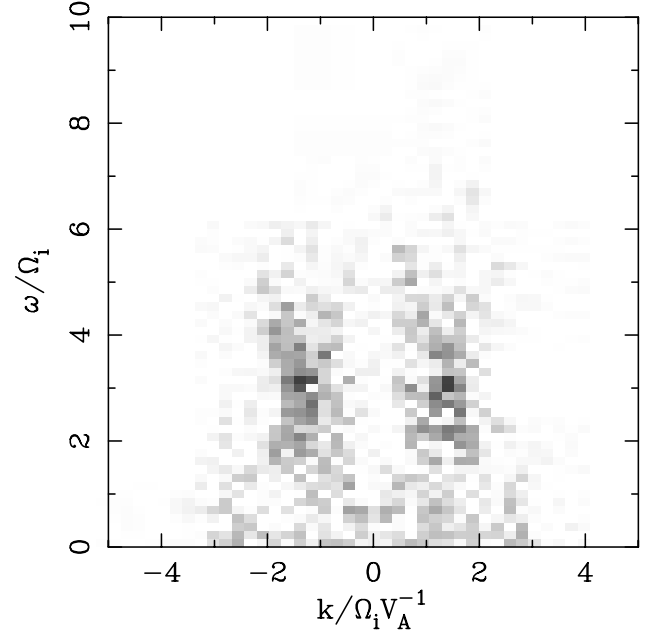perpendicular regime. Taking the value of ω with maximum power at fixed k, we then use a χ^2 best fit to derive a linear fit for the phase speed m defined from $\omega = mk$. This phase speed is shown in Fig. 5, together with the local Alfvén speed in the overshoot and downstream. Comparing these speeds and the dependence with the Mach number makes it clear that the ripple phase speed is consistent with the local Alfvén speed at the overshoot, rather than the upstream or downstream values. As can be seen from Fig. 3, the wave mode representing the ripples has a similar dispersion relation at the foot and overshoot, so the ripples at the foot are just an extension of the waves at the overshoot.

In order to look at the properties of ripples in the B_z field component, Fig. 6 shows an $\omega - k$ map for a field slice running along the overshoot of a $\theta_{B_n} = 88°$, $M_A \approx 5.7$ simulation. We see that there is no clear dispersion relation, rather just power distributed over a range of ω and k, but with a low frequency cutoff at about $\omega \approx 1.5\Omega_i$. The location of the peak in the power ($\omega \approx 3\Omega_i$) is the same as that for the B_x component.

It should be remembered that the $\omega - k$ diagrams are found by taking slices parallel to the shock surface; thus, if there are waves propagating obliquely to $\boldsymbol{B}$, then they will contribute to the $\omega - k$ map at their corresponding value of $k_\parallel$. Unless their dispersion relation depends only on $k_\parallel$, this would smear out (in ω and k) their power in the $\omega - k$ spectrum. Examining animations of the shock field components, this appears to be what is happening for the B_z spectrum (Fig. 6). There are wavefronts at an oblique angle to $\boldsymbol{B}$, predominantly in the foot and ramp regions, visible in the B_z, and also the B_y animations.

We tested the numerical dependence of our results by taking Fourier transforms of the B_x field component for two simulations, one with our standard simulation parameters and the other in which we doubled both spatial grid spacings, Δx and Δy, and the time step, Δt. If any of the properties of the ripples are dependent on numerical resolution, we would expect features of the ripples to scale with at least one of these. We found that the $\omega - k$ power maps were consistent, with both spectra showing a linear dispersion relation with a high frequency cutoff at around $|k| = 2.5\Omega_i v_A^{-1}$. The χ^2 best fit dispersion relations agreed to within 10%, which is small compared to the dramatic change in numerical resolution. Therefore, we conclude that the B_x ripples do not show significant numerical dependence.
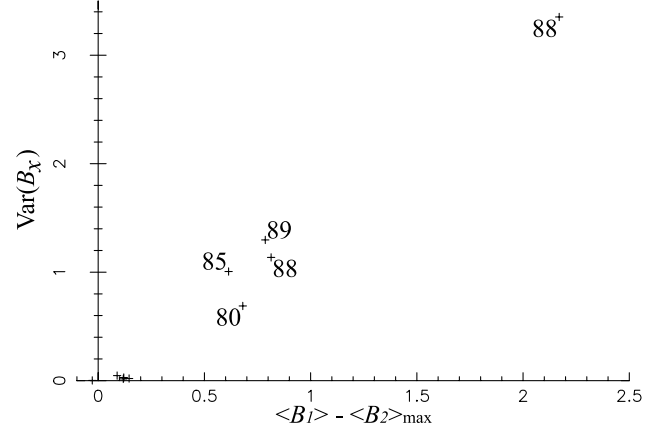
5 Ripple properties

In order to study the variation of the rippling in the x direction, we have calculated the variance of B_x, $\mathrm{Var}(B_x)$, which provides a measure of the power in the shock ripples. The quantity $\mathrm{Var}(B_x)$ at the overshoot was compared with the size of the overshoot ($\langle B_{\max}\rangle - \langle B_1\rangle_{\max}$) for a sample of 10 shocks with θ_{Bn} in the range 85°–89° and a range of Mach numbers. The quantity ($\langle B_{\max}\rangle - \langle B_1\rangle_{\max}$) is the difference between the maximum magnetic field in the shock transition and the maximum value of the downstream ($x > 5v_A\Omega_i^{-1}$) magnetic field, with both fields averaged over the y direction. This quantity gives a good idea of the size of the overshoot, compared to the downstream fluctuations and falls to approximately zero in the case of a subcritical shock, in which ion reflection is not important and there is no overshoot. This quantity depends very strongly on the inflow plasma speed, but much more weakly on θ_{Bn} over the range $\theta_{Bn} \gtrsim 80°$.
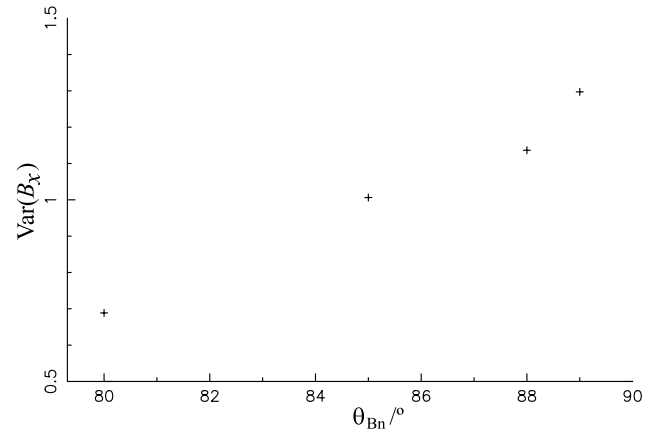
Figure 7a plots the power in the ripples against the size of the overshoot, which is related to the shock Mach number. There is a strong correlation between the two, with near zero ripple power for shocks with no overshoot. These results agree with the simulations of Hellinger and Mangeney (1997) in that the existence of ripples requires the presence of an overshoot. Figure 7b plots the power in the ripples against the angle θ_{Bn}. There is a correlation between them, with the power increasing as θ_{Bn} approaches 90°. The effect of θ_{Bn} on the strength of the shock ripples is, however, significantly less than that of the size of the overshoot.

Figure 8 shows how the variance of the magnetic field components, and, hence, the power in the ripples varies across the shock transition. The variances are plotted logarithmically, since the dynamic range is large and the dependence on x appears to be approximately exponential. The mean magnetic field strength, $\langle B\rangle$, is shown on a linear scale for comparison.

The power in B_x in the upstream region, which represents noise in the simulation, is at a low level and is approximately constant. The rise in power begins upstream of the shock foot and is approximately exponential. The small cell size in the simulations allows this exponential behaviour to be resolved.

(a) Power against size of overshoot. Labels indicate the value of θ_{Bn}.

(b) Power against θ_{Bn} for $V_{\mathrm{in}} = 4v_A$.

Fig. 7. Graphs showing how the power in the shock ripples increases with both the size of the overshoot and the value of the angle θ_{Bn}.

At a point in the shock foot the field exhibits a kink in the exponential rise, indicated by a dashed line. Downstream of this point, the exponential form continues, but the rise is less rapid. The exponential rise ends in a turnover, whose position coincides with the top of the overshoot. The power in B_x decays exponentially from this point until it reaches its downstream equilibrium value. Other supercritical shocks we have examined show similar behaviour. The B_y component also shows evidence of a kink at a similar position to the B_x kink, although the rise in power within the B_y structure is much steeper, particularly through the shock ramp. The B_z component also rises very steeply, although it contains less power than the B_x and B_y components. We also note that $\mathrm{Var}(B_z)$ does not seem to have a peak at the overshoot position.

The plasma flow speed is an interesting quantity within

(a) Var(B_x)

(b) Var(B_y)

(c) Var(B_z)
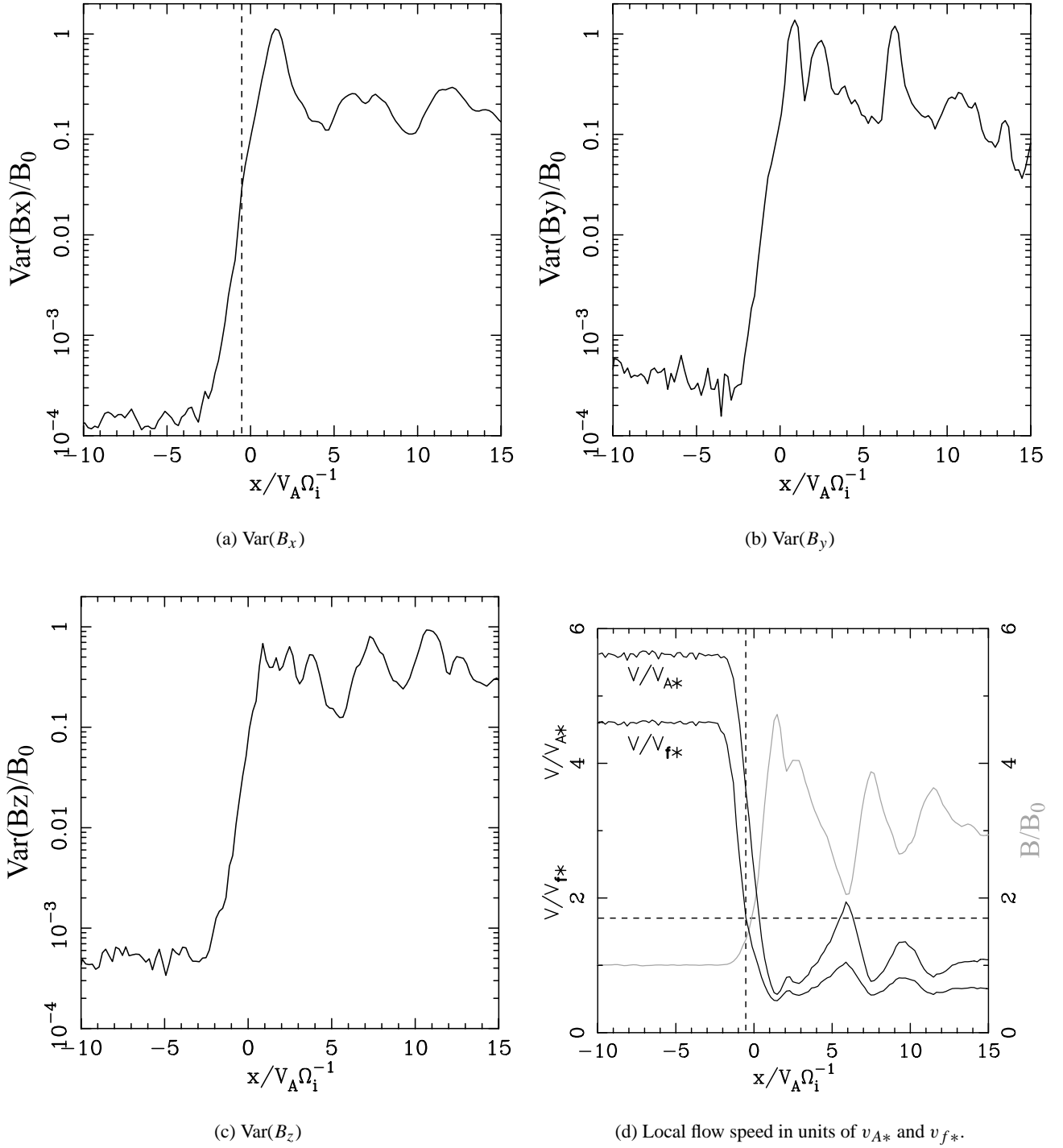

(d) Local flow speed in units of v_{A*} and v_{f*}.

Fig. 8. Variance of field components as a function of distance from the shock, for the simulation with $\theta_{B_n} = 88°$ and $M_A \approx 5.7$. The flow speed across the shock transition is also shown for comparison. The location of the kink in the B_x ripple amplitude is indicated by a dashed line.

the shock structure, particularly in relation to the kink seen in the B_x and B_y field components. The flow speed is useful in terms of the local Alfvén speed, since this is the characteristic speed for parallel propagating waves. The fast mode

transition is also of interest, since MHD waves are unable to propagate upstream of this point. McKean et al. (1995) report an ion temperature increase at the overshoot by a factor of around fifty over the upstream value, which is consistent
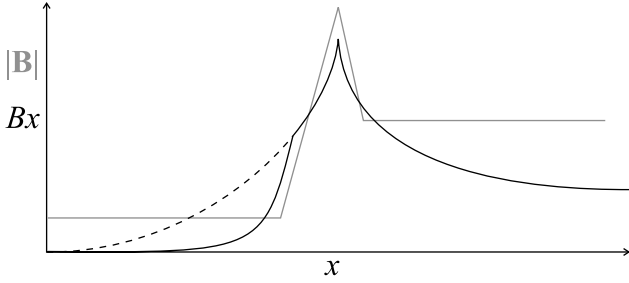
Fig. 9. A sketch of our model for a shock surface wave. The surface mode consists of a pair of exponential solutions which meet at the top of the overshoot. At a point upstream of the overshoot, the local flow velocity exceeds the local fast mode wave speed and the surface mode's exponential solution (dotted line) decays more rapidly.

with our temperature diagnostics. This results in a fast mode wave speed at the overshoot of $v_f \approx 4v_A$. We denote these local wave speeds with a star, in order to distinguish them from their upstream counterparts. Figure 8d shows graphs of the average of the x component of the plasma flow speed in the shock rest frame as a function of x in terms of the local Alfvén and fast mode wave speeds.

A comparison of Figs. 8a and b with Fig. 8d shows that the position of the kink in the B_x and B_y power graphs corresponds to a point just upstream of the super-fast transition. This transition occurs near the top of the shock foot, with the Alfvénic transition occurring further downstream near the overshoot. The positions of the fast mode and Alfvénic transitions are not dramatically different, but the position of the kink in the B_x power is closer to the fast mode transition. By doing a similar analysis for a sample of three supercritical shocks, we found that the flow speed at the kink in units of the fast mode wave speed was consistent between the simulations and averaged to $1.3v_{f*}$, whereas the flow speed in units of the Alfvén wave speed varied between $2.4v_{A*}$ and $4.0v_{A*}$. This suggests that the kink is related to the super-fast, rather than the Alfvén transition.

6   Shock surface modes

We argue that collisionless shocks may be able to support a surface mode. There has been little investigation of surface waves on shocks, so we review here the relevant issues. The existence of a surface mode at tangential discontinuities is described by Hollweg (1982). His analysis consists of considering the MHD equations and making a number of simplifying assumptions. He considered a cold plasma, with constant density and field magnitude across the discontinuity. The regions on either side of the discontinuity are homogeneous, and the discontinuity consists only of a change in the magnetic field direction. The surface mode is then identified by matching exponential solutions on either side of the discontinuity and introducing a boundary at infinity at which

the wave amplitude goes to zero. This has the effect of constraining the solution to the region of the discontinuity.

A surface mode analysis is significantly more difficult for the discontinuity at a shock overshoot, particularly as a result of the flow across the discontinuity. This is further complicated by the fact that the density, flow velocity and magnetic field strength are all strong functions of position. In the case of a collisionless shock, we treat the discontinuity surface as being the top of the overshoot, with the upstream region being that portion of the shock ramp lying between the top of the overshoot and the super-fast transition. Upstream of this point, the flow speed is greater than all MHD wave speeds. This transition could correspond with the kink that we observe in the B_x field component. A schematic view of our model is shown in Fig. 9. Although an exponential profile could, in principle, also result from the spatial damping of power in a wave mode propagating away from the overshoot, this would provide no explanation for a kink correlated with the super-fast transition.

In a shock surface mode treatment, the cold plasma assumption is also questionable, since the ion temperature can increase by a factor of fifty at the overshoot (McKean et al., 1995). The nature of the discontinuity is different too. In the case of the tangential discontinuity, the direction of the magnetic field changes discontinuously. At the shock overshoot, it is the rate at which the field changes magnitude that is discontinuous. The mode described by Hollweg (1982) has a propagation velocity along the discontinuity that is determined by the wave speeds on either side of the discontinuity. Although an analytical surface mode analysis is difficult in the shock case, we would expect any surface mode to share these two properties. Since our analysis of the ripples lies in a direction that is parallel to the magnetic field, we would, therefore, expect the characteristic wave speed to be the overshoot Alfvén speed. Also, since this is a surface mode, it should decay exponentially with distance from the discontinuity. These expectations are consistent with our simulations.

The plasma at a shock is inhomogeneous in several senses. The macroscopic parameters (magnetic field, velocity profiles) are strongly inhomogeneous. The ion distribution function also varies dramatically through the shock. The question then arises whether it is possible to distinguish a surface mode from a mode which exists simply by virtue of an unstable distribution function. In the former case, the wave exists because of the inhomogeneity (discontinuity in the simple case). In the latter, the instability might not necessarily require inhomogeneity to operate. In a self-consistent shock simulation it is difficult to distinguish these two cases unambiguously. The results of our simulations are indicative of the presence of a surface mode. One way to confirm this possibility would be to carry out MHD-like simulations of a finite thickness shock with a field structure similar to that of the hybrid simulations. The existence of surface waves in such a system would then support our conclusions.

If such a mode exists in a shock, there is likely to be sufficient energy available to excite it. There is nothing to

stop the surface mode being driven by an Alfvén Ion Cyclotron instability resulting from the reflected ions, as suggested by Winske and Quest (1988), or to be connected with the oblique whistlers generated in the shock foot. More work is needed to conclusively identify the wave mode responsible for rippling in the B_x component and to determine the source of the driving energy.

7 Summary

By using Fourier Transforms to study shock rippling, we have been able to analyse the properties of the ripples without making any assumptions about the linearity of the system. The large computational box and long duration of the underlying simulations has meant that we have been able to achieve sufficient resolution to produce convincing dispersion relations for the ripples.

Our analysis has shown, for the first time, some new features of the shock ripples, as seen in the shock normal magnetic field component in two-dimensional hybrid shock simulations. The B_x ripples can have a large amplitude, exceeding the upstream value of the magnetic field. Although the amplitude of these ripples is large, we found that the presence of rippling does not have a significant impact on the average (one-dimensional) shock profile.

The Fourier analysis of the B_x ripples shows that they propagate along the shock front at the overshoot Alfvén speed. The power spectrum of the B_x ripples has a maximum at a wavelength of several ion intertial lengths, with a high frequency cutoff. The maximum power in B_z corresponds to the maximum power in B_x, although there is no straightforward correlation between the two.

The power in the ripples is a much stronger function of the size of the overshoot, and, hence, the shock Mach number, than it is of the angle θ_{Bn}. This is significant because rippling can play a major role in producing energetic electrons downstream of the shock (Lowe and Burgess, 2000), so a weak θ_{Bn} dependence means that electron acceleration can take place over a much wider range of shock parameters than suggested by simply one-dimensional acceleration models. The ripples become weaker as the inflow velocity decreases and cease to exist when the shock becomes subcritical and lacks an overshoot.

The amplitude of the ripples varies with distance in an approximately exponential manner, reaching a maximum at the overshoot. The graph of power as a function of position exhibits a kink which means that the ripple power drops off upstream of a point which approximately corresponds to the super-fast transition. This may be significant because MHD waves are unable to propagate upstream of the fast mode transition, so it might represent an upstream boundary condition for an MHD-like surface wave. It is also possible that there is a component in B_x, albeit at low amplitude, related to the oblique whistler waves, which presumably accounts for the measured Var(B_z) profile.

We argue that many of these properties are similar to the surface mode described by Hollweg (1982) at a tangential discontinuity. In particular, the propagation velocity along the discontinuity is determined by the Alfvén speed on either side of the discontinuity, in this case at the overshoot. The exponential profile is typical of surface modes, but the fact that a kink appears at the super-fast transition indicates the presence of a further boundary. Such features are to be expected, since the case of a shock is complicated significantly by the presence of a decelerating flow across the discontinuity, which crosses various characteristic velocities.

References

Fairfield, D. H.: Whistler waves observed upstream from collisionless shocks, J. Geophys. Res., 79, 1368–1378, 1974.

Hellinger, P. and Mangeney, A.: Upstream whistlers generated by protons reflected from a quasi-perpendicular shock, J. Geophys. Res., 102, 9809–9819, 1997.

Hellinger, P., Mangeney, A., and Matthews, A.: Whistler waves in 3d hybrid simulations of quasiperpendicular shocks, Geophys. Res. Lett., 23, 621–624, 1996.

Hollweg, J. V.: Surface waves on solar wind tangential discontinuities, J. Geophys. Res., 87, 8065–8076, 1982.

Krauss-Varban, D., Pantellini, F. G. E., and Burgess, D.: Electron dynamics and whistler waves at quasi-perpendicular shocks, Geophys. Res. Lett., 22, 2091–2094, 1995.

Lowe, R. E. and Burgess, D.: Energetic electrons downstream of earth's bow shock: Simulations of acceleration by shock structure, Geophys. Res. Lett., 27, 3249–3252, 2000.

Matthews, A.: Current advance method and cyclic leapfrog for 2d multispecies hybrid plasma simulations, J. Comput. Phys., 112, 102–116, 1994.

McKean, M. E., Omidi, N., and Krauss-Varban, D.: Wave and ion evolution downstream of quasi-perpendicular bow shocks, J. Geophys. Res., 100, 3427–3437, 1995.

Orlowski, D. S. and Russell, C. T.: Ulf waves upstream of the venus bow shock: Properties of one-hertz waves, J. Geophys. Res., 96, 11 271–11 282, 1991.

Orlowski, D. S., Russell, C. T., Wu, C. S., Krauss-Varban, D., Omidi, N., and Thomsen, M. F.: Damping and spectral formulation of upstream whistlers, J. Geophys. Res., 100, 17 117–17 128, 1995.

Savoini, P. and Lembege, B.: Electron dynamics in two- and one-dimensional oblique supercritical collionless magnetosonic shocks, J. Geophys. Res., 99, 6609–6635, correction: *J. Geophys. Res.*, 99, 13 401–13 402, 1994.

Thomas, V. A.: Dimensionality effects in hybrid simulations of high Mach number collisionless perpendicular shocks, J. Geophys. Res., 94, 12 009–12 014, 1989.

Winske, D. and Quest, K. B.: Magnetic field and density fluctuations at perpendicular supercritical collisionless shocks, J. Geophys. Res., 93, 9681–9693, 1988.

Wong, H. K. and Goldstein, M. L.: Proton beam generation of oblique whistler waves, J. Geophys. Res., 93, 4110–4114, 1988.